Available online at www.sciencedirect.com
ScienceDirect
Journal of the European Ceramic Society 28 (2008) 1783–1791
www.elsevier.com/locate/jeurceramsoc

Nanocrystalline ZrO_2 ceramics with idealized macropores

Hernán Santa Cruz [a,*], José Spino [a], Georg Grathwohl [b]

[a] *Institute for Transuranium Elements, Joint Research Centre, European Commission, P.O. Box 2340, D-76125 Karlsruhe, Germany*

[b] *Ceramic Materials and Components, University of Bremen, IW 3, Am Biologischen Garten 2, D-28359 Bremen, Germany*

Received 20 September 2007; received in revised form 13 December 2007; accepted 20 December 2007
Available online 4 March 2008

Abstract

Macroporous nanocrystalline 4 mol% yttria-stabilised zirconia ceramics were fabricated by a novel colloidal processing technique, using a commercially available nano-powder with modified surface and polymethylmethacrylate (PMMA) sacrificial templates as starting materials. Monolithic bodies obtained by gel-casting of nano-powder/PMMA-templates suspensions presented remarkably homogeneous microstructures after sintering characterized by grain size <200 nm, macropore diameter around 1 μm, and closed porosity varying between 10 and 20%. The achieved microstructure highly resembles the high burn-up structure of highly irradiated light water reactor UO_2 fuel, the properties of which are aimed to be assessed via the present model material. The sintering behaviour of bodies with or without macropores was compared. The sintering activation energy for dense, PMMA-free bodies was found to be as low as 157 kJ/mol suggesting grain boundary diffusion mechanism for mass transport. For the porous material, the measured sintering activation energy was even lower (129 kJ/mol).

Keywords: Calcination; Sintering; Microstructure-final; Porosity; ZrO_2 nanocrystalline

1. Introduction

High-performance ceramics with nanoscopic microstructures are highly attractive materials due to their exceptional properties. In particular, ceramics with functionalized porosities provide the technical base for a large variety of applications and effects to be used in many processes and equipment of important technologies. These include ceramic components as substrates for catalytic processes, filters and membranes for high temperature gas cleaning or molten metal filtration, gas burner media, thermal and acoustic isolation and bioceramic devices for tissue engineering or implants for bone replacement.[1–4] The porosity characteristics are spread over a wide range with porosities that can exceed 90 vol%. The pores can be open or isolated and closed with pore sizes from sub-nanometer to millimeter dimensions. The fabrication methods are correspondingly variable including replica and burnable template techniques, direct foaming processes and decomposition or dissolution reactions of phases previously incorporated in the matrix. The emerging microstructure of the porous ceramics reflects the processing method and can be tailored according to the requirements defined by the final application. Excellent recent papers and reviews are available on these processing routes[1,5] and on more focussed methods as, e.g., nanocasting for nanostructuring porous solids,[6] porous piezoelectric ceramics,[2] or other advanced techniques.[7,8a,b] In these tailored porous ceramics the adjustment and accommodation of porosity (open or closed, cellular structures, porous or dense struts and cell walls, mono- or multimodal pore size distributions) are established with the simultaneous requirement of high strength and reliability.[9] This target is favourably addressed in this work by utilising the advantages of nanocrystalline microstructures.

The objective of this work is to develop an accessible route to produce at laboratory scale defect-free monolithic ceramic specimens with tailored pore/grain microstructure. The target configuration consists of isolated individual pores of 0.5–1 μm size, immersed in a matrix of 200–300 nm size grains and porosity levels of 10–20%. This type of microstructure is of special interest in the nuclear field because of its appearance at the periphery of light water reactor UO_2 fuel at high burn-up[10] (Fig. 1). There, due to safety reasons, questions arise concerning the capability of the structure to retain the fission gases and to

* Corresponding author. Tel.: +49 7247 951 0; fax: +49 7247 951 587.
E-mail address: jrc-itu-info@ec.europa.eu (H. Santa Cruz).

0955-2219/$ – see front matter © 2008 Elsevier Ltd. All rights reserved.
doi:10.1016/j.jeurceramsoc.2007.12.028

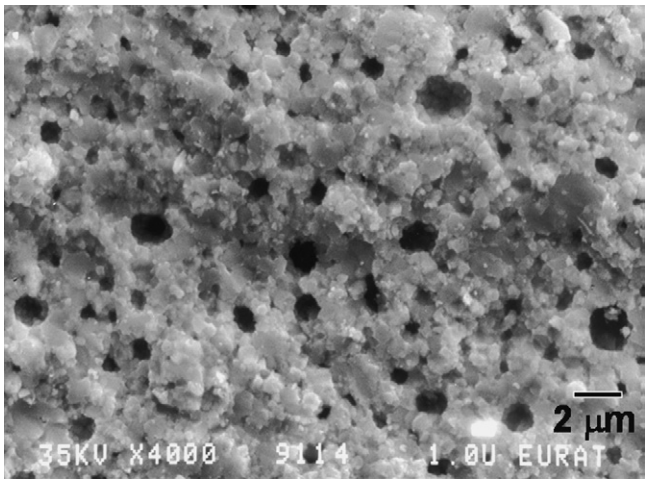

Fig. 1. Target UO_2 high burn-up structure (fresh fracture surface).

withstand peak mechanical loading under power transients. The resulting model system would enable studies of these properties with a representative, non-radioactive material.

As raw material yttria partially stabilised ZrO_2 (Y-PSZ) was selected. Y-PSZ, hitherto one of the most investigated nanocrystalline ceramic systems owing to its superplastic behaviour,[11] is also well known due to its improved mechanical behaviour through the induced transformation toughening.[12,13] The novel direct-consolidation technique developed here is based on the process of gel-casting of suspensions of commercially available Y-PSZ nano-powder. Spherical sacrificial templates of polymethylmethacrylate are co-dispersed before gelation to create the target porosity. After controlled drying of the cast gel, burn-out and sintering steps follow. Details of these steps and results of the characterization of the monolithic specimens achieved are reported in the following.

2. Experimental procedure

2.1. Materials

The fabrication of bulk ceramics was established with a 4-mol% Y-PSZ nano-powder with modified surface (12.5 wt% of 3,6,9-trioxadecanoic acid) from Buehler, Switzerland. As pore-templates, water suspensions of 1 and 2 μm monosized microspheres of polymethylmethacrylate (PMMA) with hydrophilic anionic surface (settled by $–OSO_3^-$ sulfate groups) from Micro-Particles GmbH, Berlin, Germany were utilised. As binder-additive, small quantities of a vinyl-polymer water-soluble dispersion (KB-2112) from Zschimmer & Schwarz GmbH, Lahnstein, Germany, were used.

2.2. Powder characterization

Particle size distribution and zeta-potential of the nano-powder were measured using a Malvern Zetasizer 5000 device. Powder suspensions (1 vol%) were prepared with bi-distilled water and conditioned by ultrasound for at least 5 min. The pH of the suspension was adjusted by automatic titration (Mettler DL25 Titrator) using NaOH and HCl solutions, respectively. Supplementary stability studies of dispersion series under different pH-values were performed by visual observation in transparent glass tubes. Agglomerates were destroyed by high power ultrasound (HPUS) homogenisation for a few minutes using an apparatus Sonoplus HD3200 equipped with a conic sonotrode KE76 from Bandelin.

The specific surface area (S_{BET}) of the raw powder was measured by N_2 adsorption and desorption at 77 K in a Micromeritics ASAP 2010 system, using for the evaluation the Brunauer, Emmett and Teller (BET) method.[14] An area of 0.162 nm^2 was considered for the adsorption of a N_2 single molecule. Before the measurement, the samples were degassed 24 h at 100 °C. Therewith a mean diameter D_{BET} was calculated, considering spherical particles and a Y-PSZ theoretical density (ρ) of 6.1 g/cm^3 (Eq. (1)).

$$D_{BET} = \frac{6}{\rho S_{BET}} \tag{1}$$

The crystal structure of the material before and after sintering was checked by X-ray diffraction using a Debyflex 2002 diffractometer of Seifert (θ–2θ configuration, 2θ ranging from 10° to 90°, Cu Kα radiation: $\lambda = 0.1542$ nm). The crystallite size D of the raw powder was calculated from the width of the diffraction peak W at Bragg-angle $2\theta = 30°$, using the known Scherrer expression (Eq. (2)) with Scherrer's constant K.[15]

$$D = \frac{K\lambda}{W \cos\theta} \tag{2}$$

2.3. Material characterization

Density determinations of sintered samples were carried out by the Archimedes' method in water (DIN EN 623-2), and by helium pycnometry (Micromeritics GmbH). Thermogravimetric studies (Netzsch STA 409) on green samples were carried at a heating rate 5 K/min in air or Ar-gas with 10 cm^3/min flow rate. Sintering behaviour of green samples was studied by dilatometer analysis (Baehr Thermo-analyse DIL-802). Green specimens were prepared with dimensions of 5 mm × 5 mm × 10 mm. Heating rates of 5 K/min in air atmosphere were applied. Green densities were indirectly derived from the data of the dilatometer-assays using the simplified equation (Eq. (3)) considering isotropic shrinkage, where the dependence of specimen shrinkage on time and temperature $\varepsilon(t,T)$ was converted to the relation of relative density with time and temperature $\rho_{rel}(t, T)$, with the final relative density ρ_{relf} and the final longitudinal shrinkage ε_l.[16]

$$\rho_{rel}(t, T) = \rho_{relf}\left[\frac{100 + \varepsilon_l}{100 + \varepsilon(t, T)}\right]^3 \tag{3}$$

2.4. Microstructural characterization

Fracture surfaces of the materials were characterized by scanning electron microscopy (Vega-LSH Tescan). Grain and pore size distributions were determined using UTHSCSA Image-Tool for Windows. For determination of the grain size distributions

the linear intercept procedure (ASTM E 112-88) was applied. For the pore size determination at least 100 pores were measured on each micrograph examined, calculating the individual diameters as average lengths measured in the *x*- and *y*-directions.

2.5. Submicron-grained specimens

8 mol% Y_2O_3 fully stabilised ZrO_2 (8Y-FSZ) powder from Tosoh, Japan was consolidated through centrifugal casting.[17] Specially designed flat-bottom centrifugal tubes, adapted for use in the swing-bucket rotor centrifuge *Eppendorf* 5804, were employed to obtain flat bodies. For dilatometer experiments, green specimens with dimensions of 5 mm × 5 mm × 10 mm were especially pre-formed.

3. Results

For the fabrication of the model system a 4 mol% Y-PSZ nano-powder with modified surface was employed. A specific surface area of 80 m^2/g was determined which allowed calculating a mean particle size of 12 nm. The particle size distribution of water dispersions of the powder showed diameters of d_{10} = 14 nm, d_{50} = 34 nm and d_{90} = 51 nm. The surface of the particles was chemically modified at source with a short chain organic compound (3,6,9-trioxadecanoic acid, also known as 2-[2-(2-methoxyethoxy)ethoxy]acetic acid)), which enabled the direct dispersion of the powder in water without further conditioning.

3.1. Suspension stability

The stability of low-concentrated powder aqueous suspensions was investigated in the whole pH scale. Suspensions were completely stable below pH 6. Close to the isoelectric point (IEP) at pH 8 the behaviour was completely inverted, showing immediate powder coagulation and precipitation after the addition of a basic solution (e.g. aqueous NaOH). This was due to the full elimination of the electrostatic stabilisation by neutralization of the surface charges. These conditions could also be followed by zeta-potential measurements where the zeta-potential reached values as high as 40 mV at low pH (Fig. 2). Beyond pH 6.5 the zeta-potential started to decrease continuously up to pH 12, where a minimum of −40 mV was achieved. Once coagulation and precipitation proceeded due to basic treatment it was not possible to redisperse the powder again in the high pH range. For comparison, Fig. 2 also includes zeta-potential curves of two electrostatic stabilised ZrO_2 submicron-powders (with and without yttria doping) after Pettersson.[18]

Stable suspensions with solid contents around 16 vol% (pH 2–5) turned immediately to gel-like structures on further addition of powder (visual observation of gel consistency). This behaviour may be attributed to the high organic content of the powder (i.e., 12–15 wt% related to the solid content as determined by thermo-gravimetry, confirming data of the supplier). It is assumed that close-packed powder particles interact with each other due to the short organic chains chemically adsorbed to the surface, forming a kind of network where water molecules are

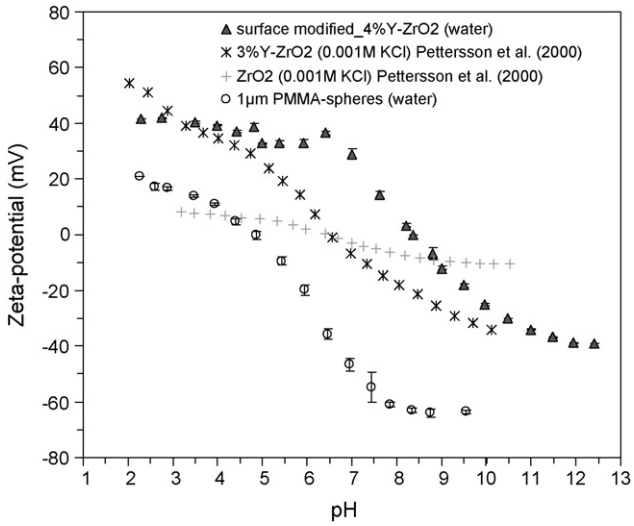

Fig. 2. Zeta-potential of ZrO_2 powders and 1 μm PMMA-spheres in water.

captured (i.e. gelation). Exploiting this characteristic of the powder, a direct forming process, similar to gel-casting[19,20] and other direct consolidation techniques was used to prepare the green bodies. Briefly, the complete colloidal processing involved the preparation of the aqueous suspension, homogenisation (deagglomeration) by HPUS and the gel-casting step, followed by humidity-controlled drying in silicon-rubber moulds. As a result completely homogeneous and mechanically resistant green bodies were obtained.

For pore formation, mono-sized PMMA beads as sacrificial templates were utilised. Water suspensions of PMMA microspheres were mixed together with the Y-PSZ nano-powder. Commercial PMMA microspheres with hydrophilic negative charged surface given by sulfate groups covalent bonded (i.e. originated from the persulfate used as initiator of polymerisation) were selected, which provided good dispersibility in the polar medium. Furthermore, below their IEP (at pH 5), PMMA microspheres showed a lower positive zeta-potential than the Y-PSZ particles (Fig. 2). Thus, the mixture of the PMMA-spheres into the suspension was easier provided due to the less strong repulsive interaction of the well-stabilised powder particles with the microbeads which would be rather surrounded, and at the same time stabilised, by Y-PSZ particles. Additionally, the relative low burn-out temperature of the PMMA (under 600 °C in air) ensures its complete elimination before the densification process is activated. This prevents samples from catastrophic rupture due to the easy gas release.

A binder additive was required as third component for the enhancement of the green body strength. For this purpose, addition of 2.5–3 wt% (referred to the solid content) of a commercially available vinyl-polymer hydrophilic binder dispersion was implemented.

For the preparation of stable suspensions the powder was carefully added to a preset PMMA/binder/water solution under continuous agitation. Owning to the acidic character of the surface modifier supplied with the powder, the pH of the suspension was auto-regulated in the stable acidic region directly by the addition of the nano-powder (pH∼2–3). No further pH

adjustments were required. Flocks or light agglomerates were destroyed by HPUS conditioning. The heat transmitted to the suspension during the HPUS treatment favoured further the homogenisation of the mixture.

3.2. Critical step: drying

Immediately after HPUS the aqueous powder-PMMA dispersion was poured into silicon-rubber moulds for shaping and drying. The lower viscosity caused by the higher temperatures during ultrasound processing enabled a more efficient casting including the faster migration of residual bubbles to the top of the solution by enhanced flotation–separation. As a function of time and temperature reduction the casted suspension turned to a rigid body. The drying process was found to be a first critical step, since crack-formation occurred at ambient temperature and humidity conditions (i.e., 20–25 °C and <50% RH). An extremely fast drying rate was observed on the surface of the compacts just after casting of the suspension. Thereafter the dried surface blocked the diffusion paths for water molecules. Consequently, density gradients inside the body generated stresses leading finally to cracks. Therefore, a long-term (8–10 days) humidity-controlled drying process at room temperature was implemented. For this purpose, a humidity-controlled chamber under continuous air transfer (under slightly reduced pressure) was established. Two magnetic valves, controlled by a humidity-transmitter (TH200 from Kimo Instruments) with remote sensor positioned inside the chamber, enabled the entrance of wet or dry air, respectively. Initial high humidity (>95% RH) setting avoided a sealing effect of the surface. The humidity setting was sequentially lowered (at least after each 48 h) until the external room humidity conditions were reached (approximately 50% RH). After drying, defect-free green parts were obtained.

First attempts to employ the method with powder suspensions led to green compacts with very weak intrinsic bonding forces. This was attributed to the strong polar character of the organic surface-modifier that caused repulsive interactions among particles, whose lack of adherence remained in the dried compact, therefore favouring crack propagation. The addition of very low concentrations of hydrophilic binder enhanced the bonding forces within the green compact, promoting a crack-free drying. So, it was possible to pre-form the compacts in the desirable shape by cutting and grinding before sintering. A further obstacle caused by the highly polar surface modification of the powder was the adhesion of the dried compact to several mould materials tested. This frequently provoked cracking during drying or during de-moulding. After trials with different compositions, it was found that strong hydrophobic materials, such as silicon rubber, worked efficiently avoiding adhesion between compact and mould. Dried specimens suffered a total macroscopic shrinkage of 12–18% at the end of the process.

SEM micrographs of the green compact (Fig. 3) showed how the PMMA-microspheres are inserted in the fine-grained solid-organic matrix. Some microbead shrinkage after drying was observed. However, the PMMA contraction was found favourable, since this non-rigid behaviour avoided the formation

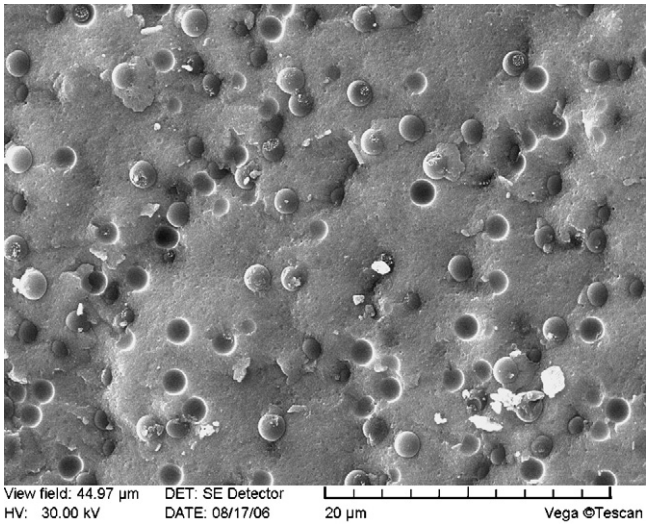

Fig. 3. Green body with 2 µm spheres (PMMA) dispersed in the nano-grain matrix.

of cracks due to the absence of tensile stresses in the matrix.[21] No density gradients of templates were observed in the cross-sections analysed by SEM, showing in all cases a homogeneous microstructure.

Green density determinations (excluding additives) revealed 42–45% of the Y-PSZ theoretical density (TD) for PMMA-free bodies and 37–38% TD for PMMA-containing compacts.

3.3. Critical step: burn-out

The burn-out of additives in the dried specimen was found to be the second and most challenging critical step of the process due to the high volume fraction of organics involved. Formation of macro-cracks due to blocked diffusion paths, which hindered the release of the abundant gas molecules generated during the thermal decomposition of the additives, appears as the main limitation of the insufficiently controlled fabrication process.

The burn-out was investigated for different atmospheres and heating rates. It was observed that the flow rate of the ambient gas had an important impact on the microstructure. Thus, if the flow rate was low, a distribution of new cracks with the form of a "honeycomb" appeared. This crack pattern can be attributed to the lower diffusion rate of the generated gas molecules towards the bulk surface compared with their formation rate. The internal gas pressure forces then the material to crack, and burst-venting of the accumulated gases is likely to occur. For PMMA-free specimens, higher gas flow rates reduced, but did not completely eliminate the formation of cracks.

On the contrary, for any gas flow rate, bodies containing PMMA beads showed an improved behaviour with any crack formation during organics burn-out. The mass change and, concurrently, the shrinkage of these samples were investigated by differential dilatometry (D-DIL) and differential thermo-gravimetry (D-TG). The resulting curves revealed under constant heating rate conditions (5 K/min) in air two decomposition peaks (mass-loss/shrinkage) in the temperature range 200–400 °C (Fig. 4). According to D-TG the first decompo-

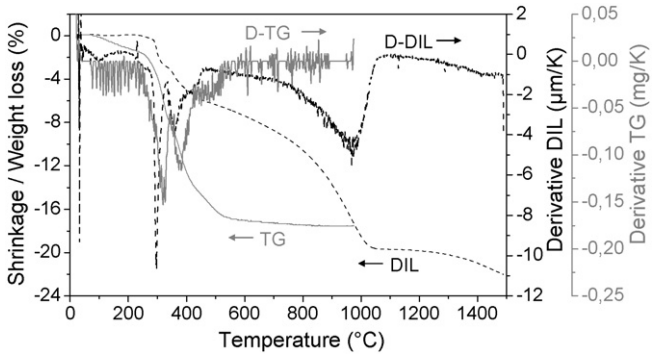

Fig. 4. Thermo-gravimetry (TG) and derivative TG (D-TG) (continuous lines), as well as dilatometry (DIL) and derivative DIL (D-DIL) (dashed lines) of Y-PSZ/PMMA bodies. Test conditions: heating rate 5 K/min, in air with flowing rate of 10 cm^3/min.

sition step started at around 240 °C with a maximum rate at 330 °C followed by the second decomposition process with a maximum rate at 380 °C. The D-DIL curve showed the same two peaks (in this case indicating shrinkage), though shifted by about 10–20 °C towards lower temperatures. Separate D-TG tests confirmed that the first peak observed was caused by the thermal decomposition of the surface modification additive of the powder (3,6,9-trioxadecanoic acid) and that the second one corresponded with the elimination of the PMMA microspheres. The shrinkage accompanying the trioxadecanoic acid decomposition is especially significant and thus assigned as the principal cause for crack formation during calcination. The shrinkage rate of the second step is of lower extent not contributing to crack formation. This demonstrates the excellent performance of the PMMA-spheres as templates for the porosity, i.e. avoiding any critical stresses for crack formation in the material. Similar experiments were performed in Ar-gas. It was shown that compared to the burn-out in air all the above-mentioned peaks were displaced by about 10–30 °C to higher temperatures. The form of the curves remained, however, unchanged. In view of these results, it was decided to perform the burn-out treatment in air at very low heating rates (<0.2 K/min in the most critical temperature intervals) to avoid strong exothermic reactions. The only disadvantage of this method was the long burn-out period required for the production of defect-free bodies.

It can be assumed that the beneficial effect of PMMA-filler during the critical burn-out process is related to the influence of this disperse template phase on the emerging microstructure. This influence can be seen in the hindered shrinkage of the matrix which leads to an increased void volume between the templates at the beginning of the burn-out process. Additionally, this effect may be enhanced by a pore stabilisation mechanism. The volume fraction of the filler beads offers an intermediate reservoir for the gaseous products to be released thereby, reducing the internal gas pressure and thus stabilising the whole macro-structure. A schematic model for this process is represented in Fig. 5. The premise here is that the out-diffusing gas from burn-out travels only short distances until falling trapped in partially emptied cavities working as interim gas reservoirs.

Once the organics are completely decomposed the highly coordinated pores, surrounded by large numbers of grains, may form very stable cavities where the gas is effectively retained. Hence, slightly pressurized pores due to the retained gases arising from burn-out might be expected in samples prepared with the fillers under these conditions.

3.4. Sintering and microstructure

The D-DIL curves (Fig. 4) show that the nano-scale material starts noticeable sintering at very low temperatures, i.e., as low as 700 °C or below, with the maximum sintering rate at around 980 °C. This temperature is clearly lower than that for standard micrometer-grained ceramics.

By dilatometer studies it was also possible to determine the activation energy of the sintering process. This investigation was performed following the non-isothermal method of Young and

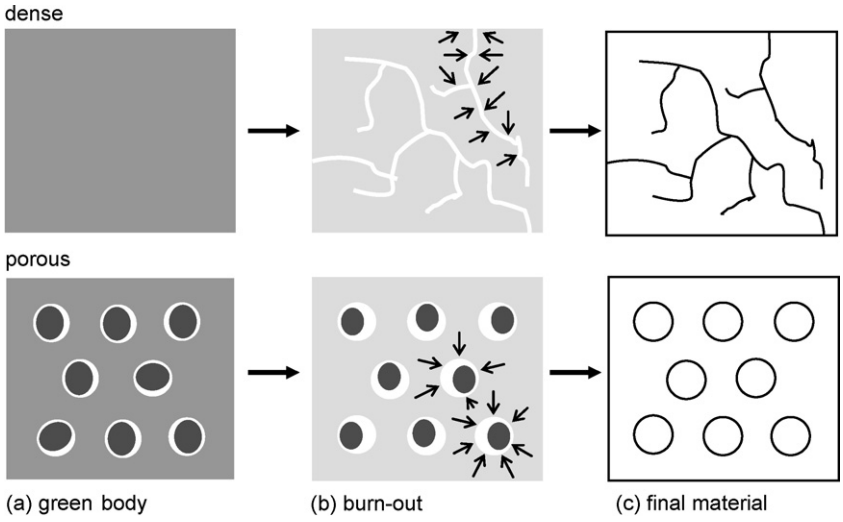

Fig. 5. Schematic model of gas release process in a PMMA-free sample leading to a network of cracks (upper row) and (with PMMA) in crack-free macroporous body (lower row) (small arrows in the figure indicate dominant intermediate position of the gas).

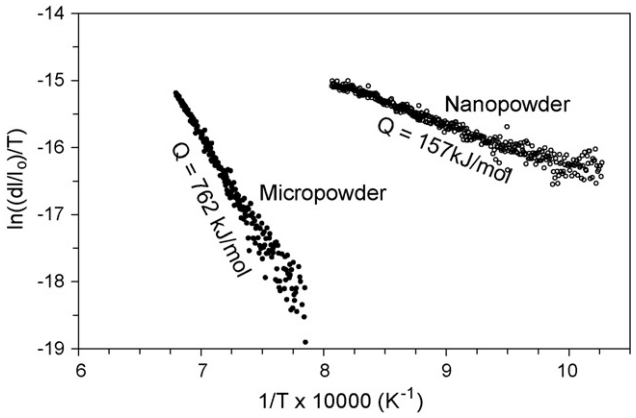

Fig. 6. Arrhenius plot of the initial densification stages for a nanocrystalline material fabricated by gel-casting (open circles) compared with a submicron material fabricated by centrifugal casting (closed circles).

Cutler[22] (Eq. (4)):

$$\frac{\Delta l/l_0}{T} = \text{const} \times \exp\left(\frac{-nQ}{\text{RT}}\right) \quad (4)$$

where n is a constant characteristic for the sinter mechanism, Q is the apparent activation energy for densification, $\Delta l/l_0$ is the relative shrinkage and RT has its usual meaning. The Arrhenius plot of these results is shown in Fig. 6. In order to be able to compare these results with literature data, arbitrary diffusion coefficients were assumed. Taking $n = 1/3$ (grain boundary diffusion), activation energies Q of 157 and 129 kJ/mol were calculated for the sintering of the nano-powder, using PMMA-free and macroporous (from PMMA-templates) compacts, respectively. The same experiment was carried out with an 8Y-FSZ submicrometer-sized powder, consolidated by centrifugal casting as described in Ref.[17] For this powder an activation energy of 762 ± 35 kJ/mol was determined (Fig. 6), which agrees well with values published in the literature for large grained samples (736 kJ/mol[23,24]). The temperature ranges where these densification mechanisms were activated differ considerably with 700–980 °C for the nano-powder compared with 1000–1200 °C for the micro-powder (Fig. 6). The more than four times lower activation energy of the nano-powder is doubtless originating from its extremely small particle size. One effect of the phenomenon can be seen in the extremely large density of grain boundaries and triple points of the nano-grain compact, in which the diffusion proceeds faster than in more conventional microstructures.[25] A second aspect contributing to the lower activation energy was postulated by Theunissen[26] describing a particle reorganization process.

The microstructure achieved after sintering at 1000 °C for 2 h is presented in Fig. 7. Though incomplete sintering, the sample exhibited a well-densified matrix with nanocrystalline grains of size ~70–80 nm. As expected, the tailored pores introduced by PMMA templates (in this case 2 μm initial size) were perfectly spherical. A small amount of 100–200 nm size pores was additionally observed, which was attributed to the burn-out of the binder-additive. This undesired porosity, with a remnant fraction of 4% at 1200 °C, impeded the achievement of fully dense bodies, though without any influence on the macro-porosity.

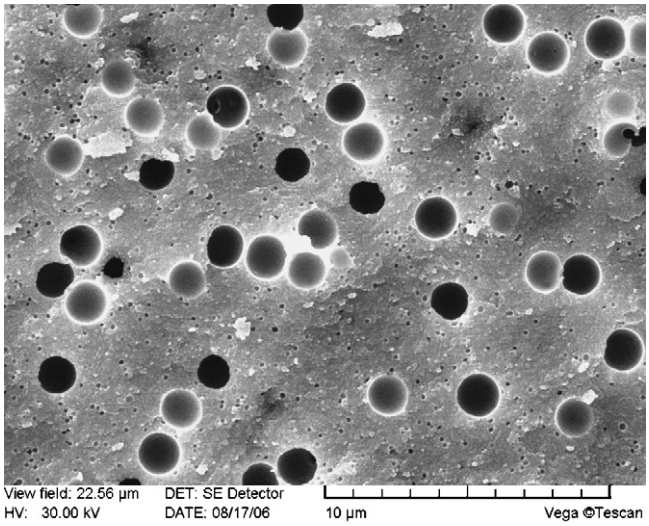

Fig. 7. Fracture surface of a sintered body fabricated by gel-casting with 2 μm PMMA templates after sintering at 1000 °C for 2 h. Beside the templated macropores, spurious residual pores (100–200 nm) are observed caused by the binder burn-out.

A homogeneously distributed macro-porosity, tailor-made with respect to the spherical shape and isolation of the pores, has been achieved with volume fractions beyond 20% after 4 h sintering at 1200 °C (Fig. 8). The total and closed porosities decreased with higher sintering temperatures revealing a very small fraction of open porosity for the samples containing macropores (Fig. 9). The almost coincidence of the total and closed porosity values is noticeable for the samples without PMMA-templates.

In Fig. 10, the microstructure (fracture surface) obtained for a porous sample sintered at 1320 °C for 1 h is shown at different magnifications. In this case the body was prepared with 1 μm

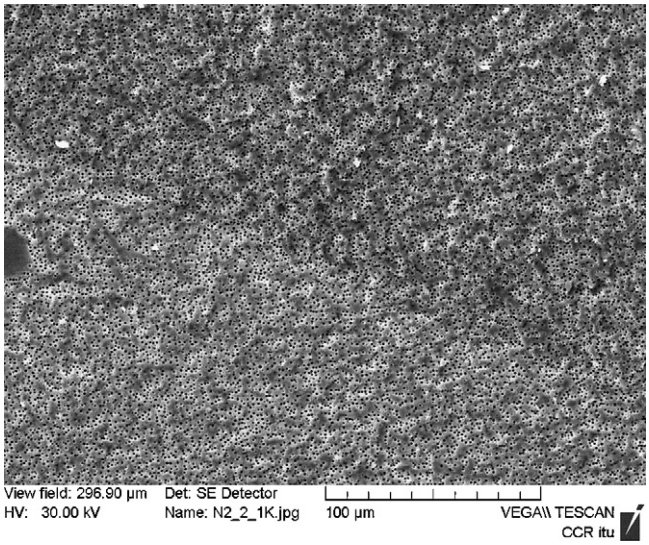

Fig. 8. Fracture surface of a sintered body fabricated by gel-casting with 2 μm PMMA templates after sintering at 1200 °C for 4 h. Porosity fraction >20% (initial PMMA fraction ~39 vol%).

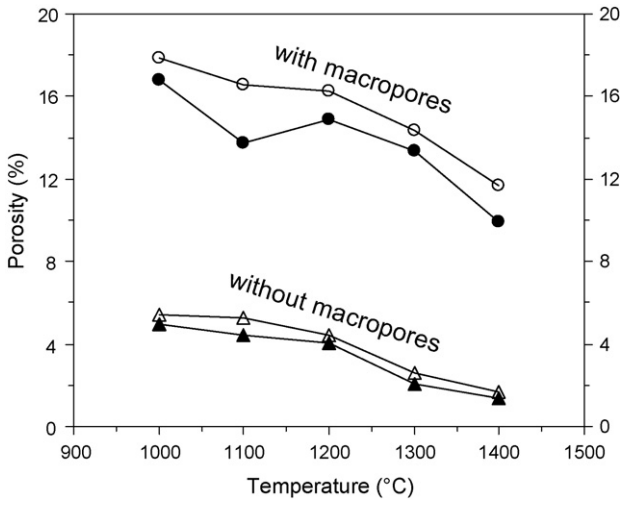

Fig. 9. Evolution of total porosity (open symbols) and closed porosity (closed symbols) of samples with and without templated macropores (initial PMMA fraction ~24 vol%) sintered 4 h at different temperatures.

size sacrificial templates using no binder-additive. Nanometer-sized pores (<200 nm) are not observed. The microstructure is characterized by 200 nm grains and pore sizes around 500 nm, with a total porosity of approximately 10%. The pores are perfectly closed, surrounded by 10–14 grains (2D image) and immersed in a fully dense-packed matrix (Fig. 10). The resulting microstructure resembles with striking fidelity the target high burn-up structure (HBS) observed in nuclear fuels[10] (Fig. 1).

It is known that small crystallites of partially stabilised ZrO_2 can retain their structure on cooling over the tetragonal/monoclinic (t–m) phase transition, producing toughening mechanisms of the material due to a stress-induced martensitic transformation (transformation toughening).[27–29] For lower yttrium contents, spontaneous transformation to the monoclinic phase can occur (understabilisation), causing mechanical degradation (micro-cracking) of the material. The present material contained nominally 4 mol% of Y_2O_3. However, it is suspected that the yttrium content at the surface of the powder could have been lowered by acid dissolution[30] since the powder was suspended in a very acidic medium (pH~2–3) for a relative long

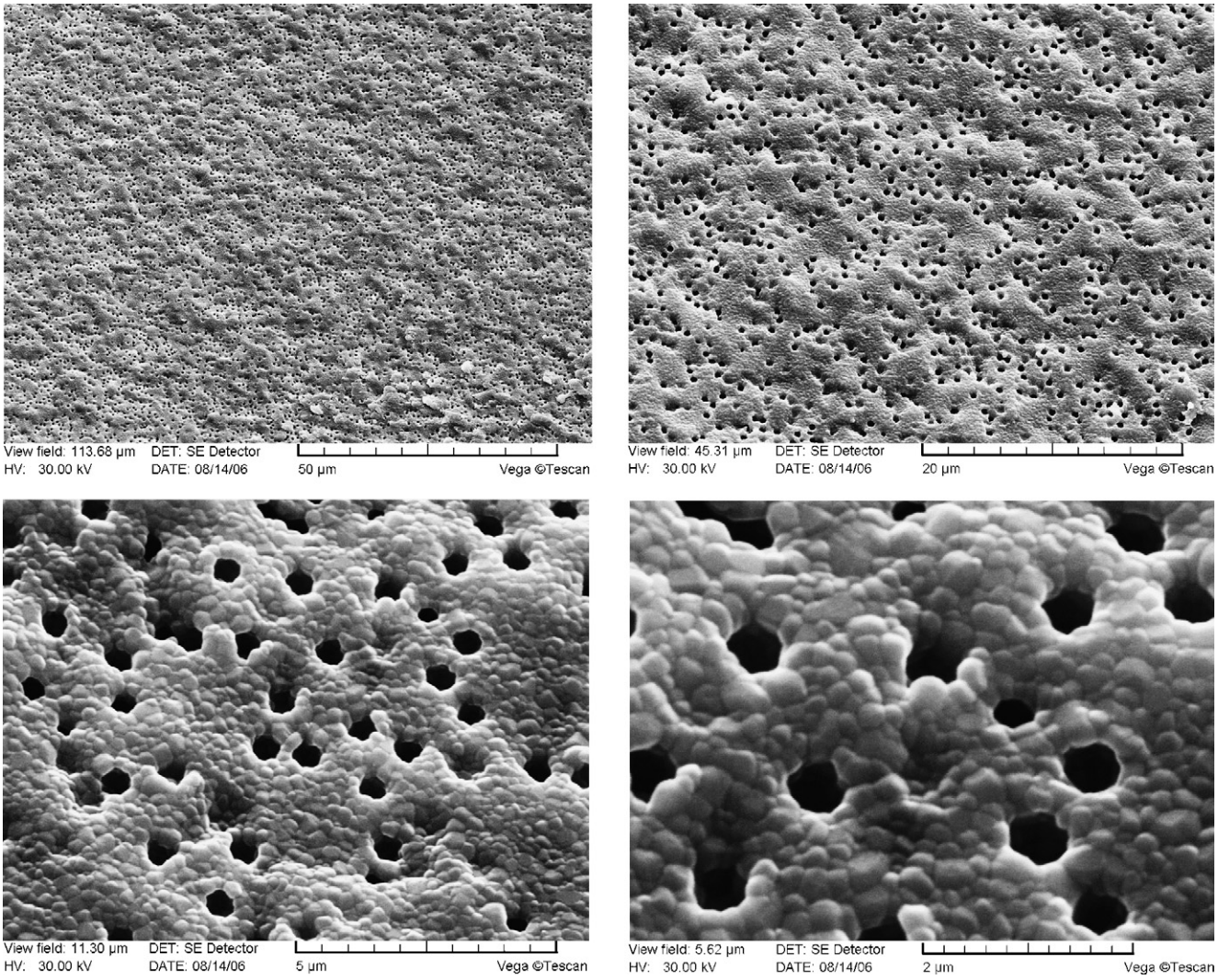

Fig. 10. Fracture surface of a sintered body fabricated by gel-casting and containing 1 µm PMMA templates after sintering at 1320 °C for 1 h. Mean grain size 200 nm, mean pore size 460 nm, ~10% porosity.

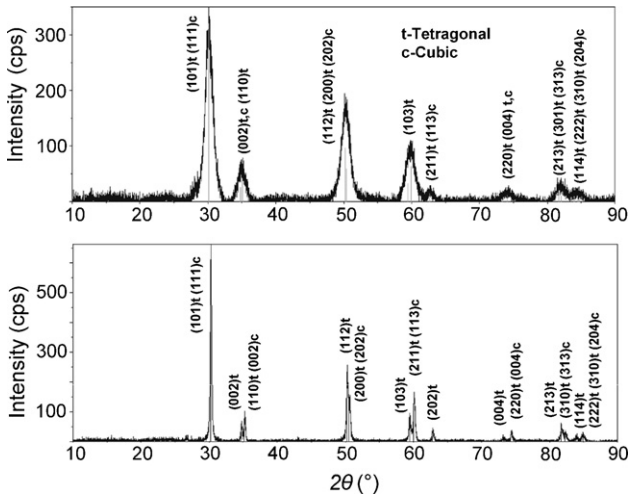

Fig. 11. X-ray diffraction patterns for ZrO_2: raw powder (above) and sintered material (below).

period of time (yttrium is soluble in acid media). The low pH of the suspension was caused by the highly acid character of the surface modification.

Therefore, to exclude possible crack formation caused by preparation-induced understabilisation, X-ray diffraction (XRD) patterns of the 4 mol% Y-PSZ raw powder and of samples sintered at temperatures of 1000, 1200 and 1300 °C were investigated. Fig. 11 shows the XRD diffractograms of the raw powder and of a sample sintered at 1300 °C, in which no sign of the monoclinic phase is present. Samples sintered at other temperatures showed likewise no evidence of the monoclinic phase. As for the raw material, a crystallite size <10 nm was calculated using Scherrer's equation for the characteristic peak at diffraction angle $2\theta = 30°$. For the severest case of the sample treated at 1300 °C for 1 h, the mean grain size was <200 nm as observed by SEM. Beside the typical enhanced sharpness of the diffraction lines in the sintered samples (through structure definition and crystallite enlargement), a slight shift towards higher Bragg-angles was detected, suggesting a minor decrease of the lattice constant (Fig. 11). This indicated a small loss of Y_2O_3 during the process (the lattice spacing increases with the Y_2O_3-content[31]). However, since the derived Y_2O_3-loss was minor and the crystallite size (<200 nm) was well below the threshold dimension for spontaneous t–m transformation (for 4 mol% Y-PSZ: $\geq$1 μm[29]), no transformation-induced cracking of the present material needs to be taken into account.

4. Discussion

The present work was focused on the production of bulk nanocrystalline materials with tailored random micrometer-sized porosity. The established colloidal processing technique for fabrication of nanocrystalline materials was extended to a modified gel-casting process, which can be described as casting of highly concentrated and ordered suspensions. This gel-casting process adapted did not follow a conventional gelation step, as, e.g., by applying temperature change conditions, to achieve fast solidification of the compact.[32] On the contrary, long-term drying under controlled humidity conditions was here applied with the object of completely avoiding any density gradients and surface sealing. Highly concentrated colloidal suspensions could be conditioned for this purpose, where the particles were extremely ordered, and gelation could easily be obtained just by increasing the solid concentration. Further organization and compaction of particles, e.g., by gravitational sedimentation is then avoidable and ideal packing is achieved as it is the case for example in the float packing process of low-concentrated dispersions described elsewhere.[33] Similarities with direct coagulation casting (DCC)[34] could be found as well, nevertheless in our case no de-stabilisation and flocculation of the suspension occurs, on the contrary, particles remain rather stabilised during the whole process. In the present case, as the particles were assumedly already close-packed in a pre-form of the gel structure, the key step to produce a homogeneous high-density network was the slow elimination of spacer molecules (i.e., water and organics) located in the void spaces between the particles. Similar processes, as, e.g. applied to the fabrication of highly ordered photonic crystals by hetero-coagulation of templates,[35] do not lead reportedly to mechanically resistant bulk ceramics. Besides, an additional step for the consolidation (e.g. pressure filtration or sedimentation) is normally required, which is not necessary in the present case.

The fact that the powder is composed of primary particles which are chemically modified by short organic chains, enables the perfect stabilisation of the suspensions, due to a highly effective electrosteric interaction. However, a principal disadvantage of the nano-powder used is its large free surface, which greatly increases the organic fraction required to achieve the perfect stabilisation (i.e. via complete coverage of the surface by an organic monolayer). Another associated drawback is the described, otherwise advantageous tendency to form pastes by premature gelation, which limits the maximum solid content in the dispersion, making more difficult the drying and consolidation processes. Notwithstanding these difficulties, the resulting microstructure is very close to the target one.

5. Conclusion

The achieved microstructure via the reported gel-casting process resembles very closely the HBS target material. The selected commercial raw materials (powder and PMMA-microspheres), as well as the developed processing method, are found adequate for the accomplishment of the desired microstructure. Macroporous monolithic samples of nanocrystalline stabilised ZrO_2 could be successfully fabricated at laboratory scale. However, scale-up of this method for the production of samples with larger dimensions is limited first by the required slowness of the drying process and second by the extremely delicate burn-out step. Nevertheless, despite the high amount of organic mass to be removed during thermal decomposition of additives, an improved burn-out process was established for the macroporous/nanocrystalline bodies based on the increased void volume of the matrix due to the hindered shrinkage by the PMMA-template filling. Additionally, a pore stabilisation effect is proposed which may allow interme-

diate storage of gases in the templated cavities during burn-out, thus, greatly reducing the internal pressure and the propensity for cracking. Furthermore, PMMA templates were found to be highly suitable for the production of tailored porosity due to their elasticity and lack of adhesion to the matrix material. In all samples a closed-cell porosity type was confirmed after sintering with a volume fraction very close to the total porosity measured. A very low sintering activation energy for the nano-powder was found. The porous specimens showed a light tendency to an even further reduced sintering activation energy. The correspondingly measured sintering activation energy for a reference micro-powder, which was in agreement with the literature values, was about five times larger than the nano-powder. The enormous densification activity of the nano-powder with enhanced surface and grain boundary diffusivities is thereby manifested.

Acknowledgments

This research was supported by the European Commission, within the frame of the Institutional Work Action Program Safety of Conventional Nuclear Fuels.

Our thanks to Thierry Wiss and Hartmut Thiele (Institute for Transuranium Elements (ITU)) for the support with SEM, and Lars Henkel (Ceramic Materials and Components, University of Bremen) and Said Yagoubi (ITU) for help with XRD-measurements and XRD-data interpretation.

References

1. Studart, A. R., Gonzenbach, U. T., Tervoort, E. and Gauckler, L. J., Processing routes to macroporous ceramics: a review. *J. Am. Ceram. Soc.*, 2006, **89**(6), 1771–1789.
2. Galassi, C., Processing of porous ceramics: piezoelectric materials. *J. Eur. Ceram. Soc.*, 2006, **26**(14), 2951–2958.
3. Gain, A. K., Song, H.-Y. and Lee, B.-T., Microstructure and mechanical properties of porous yttria stabilized zirconia ceramic using poly methyl methacrylate powder. *Scripta Mater.*, 2006, **54**(12), 2081–2085.
4. Rezwan, K., Chen, Q. Z., Blaker, J. J. and Boccaccini, A. R., Biodegradable and bioactive porous polymer/inorganic composite scaffolds for bone tissue engineering. *Biomaterials*, 2006, **27**, 3413–3431.
5. Colombo, P., Conventional and novel processing methods for cellular ceramics. *Philos. Trans. Royal Soc. A*, 2006, **364**, 109–124.
6. Lu, H.-A. and Schüth, F., Nanocasting: a versatile strategy for creating nanostructured porous materials. *Adv. Mater.*, 2006, **18**, 1805–1973.
7. Garrn, I., Reetz, C., Brandes, N., Kroh, L. W. and Schubert, H., Clot-forming: the use of proteins as binders for producing ceramic foams. *J. Eur. Ceram. Soc.*, 2004, **24**, 579–587.
8. (a) Lavrentyeva, O. and Grathwohl, G., Zellularkeramik aus autarken Schäumungsprozessen keramischer Suspensionen, Teil 1. *Keramische Zeitschrift 2*, 2007, **59**, 88–93;
   (b) Lavrentyeva, O. and Grathwohl, G., Zellularkeramik aus autarken Schäumungsprozessen keramischer Suspensionen, Teil 2. *Keramische Zeitschrift 4*, 2007, **59**, 260–265.
9. Gibson, L. J. and Ashby, M. F., *Cellular Solids, Structure and Properties* (*2nd ed.*). Cambridge University Press, Cambridge, UK, 1999.
10. Spino, J., Vennix, K. and Coquerelle, M., Detailed characterisation of the rim microstructure in PWR fuels in the burn-up range 40–67 GWd/tM. *J. Nucl. Mater.*, 1996, **231**(3), 179–190.
11. Wakai, F., Sakaguchi, S. and Matsuno, Y., Superplasticity of yttria-stabilised tetragonal ZrO_2 polycrystals. *Adv. Ceram. Mater.*, 1986, **1**(3), 259–263.
12. Garvie, R. C., Hannink, R. H. and Pascoe, R. T., Ceramic steel? *Nature*, 1975, **258**, 703–704.
13. Swain, M. V., Grain-size dependence of toughness and transformability of 2 mol% Y-TZP ceramics. *J. Mater. Sci. Lett.*, 1986, **5**, 1159–1162.
14. Brunauer, S., Emmett, P. H. and Teller, E., Adsorption of gases in multimolecular layers. *J. Am. Chem. Soc.*, 1938, **60**(2), 309–319.
15. Cullity, B. D., *Elements of X-Ray Diffraction*. Addison-Wesley Publishing Company, Inc., Reading, MA, USA, London, England, 1959.
16. Maca, K. and Simonikova, S., Effect of sintering schedule on grain size of oxide ceramics. *J. Mater. Sci.*, 2005, **40**, 5581–5589.
17. Huisman, W., Graule, T. and Gauckler, L. J., Centrifugal slip casting of zirconia (TZP). *J. Eur. Ceram. Soc.*, 1994, **13**(1), 33–39.
18. Pettersson, A., Marino, G., Pursiheimo, A. and Rosenholm, J. B., Electrosteric stabilization of Al_2O_3, ZrO_2, and 3Y-ZrO_2 suspensions: effect of dissociation and type of polyelectrolyte. *J. Colloid Interf. Sci.*, 2000, **228**(1), 73–81.
19. Omatete, O. O., Janney, M. A. and Strehlow, R. A., Gelcasting—a new ceramic forming process. *Ceram. Bull.*, 1991, **70**(10), 1641–1649.
20. Omatete, O. O., Janney, M. A. and Nunn, S. D., Gelcasting: from laboratory development toward industrial production. *J. Europ. Ceram. Soc.*, 1997, **17**(2–3), 407–413.
21. Mattern, A., Huchler, B., Staudenecker, D., Oberacker, R., Nagel, A. and Hoffmann, M. J., Preparation of interpenetrating ceramic–metal composites. *J. Eur. Ceram. Soc.*, 2004, **24**(12), 3399–3408.
22. Young, W. S. and Cutler, I. B., Initial sintering with constant rates of heating. *J. Am. Ceram. Soc.*, 1970, **53**(12), 659–663.
23. Maca, K., Trunec, M. and Dobsak, P., Bulk zirconia nanoceramics prepared by cold isostatic pressing and pressureless sintering. *Rev. Adv. Mater. Sci.*, 2005, **10**, 84–88.
24. Shojai, F. and Mäntylä, T. A., Effect of sintering temperature and holding time on the properties of 3Y-ZrO_2 microfiltration membranes. *J. Mater. Sci.*, 2001, **36**(14), 3437–3446.
25. Gleiter, H., Nanocrystalline materials. *Prog. Mater. Sci.*, 1989, **33**(1), 223–315.
26. Theunissen, G. S. A. M., Winnubst, A. J. A. and Burggraaf, A. J., Sintering kinetics and microstructure development of nanoscale Y-TZP ceramics. *J. Eur. Ceram. Soc.*, 1993, **11**(4), 315–324.
27. Claussen, N., Fracture toughness of Al_2O_3 with an unstabilized ZrO_2 dispersed phase. *J. Am. Ceram. Soc.*, 1976, **59**, 49–51.
28. Evans, A. G. and Heuer, A. H., Review-transformation toughening in ceramics: martensitic transformations in crack-tip stress fields. *J. Am. Ceram. Soc.*, 1981, **63**, 241–248.
29. Lange, F. F., Transformation toughening (Parts 1and 3). *J. Mater. Sci.*, 1982, **17**(1), 25–234 and 240–246.
30. Greenwood, R. and Kendall, K., Acoustophoretic studies of aqueous suspensions of alumina and 8 mol% yttria stabilised zirconia powders. *J. Eur. Ceram. Soc.*, 2000, **20**(1), 77–84.
31. Lamas, D. G. and Reca, N. E. W. D., X-Ray diffraction study of compositionally homogeneous, nanocrystalline yttria-doped zirconia powders. *J. Mater. Sci.*, 2000, **35**, 5563–5567.
32. Santacruz, I., Nieto, M. I. and Moreno, R., Alumina bodies with near-to-theoretical density by aqueous gelcasting using concentrated agarose solutions. *Ceram. Int.*, 2005, **31**(3), 439–445.
33. Godlinski, D., Kuntz, M. and Grathwohl, G., Transparent alumina with submicrometer grains by float packing and sintering. *J. Am. Ceram. Soc.*, 2002, **85**(10), 2449–2456.
34. Gauckler, L. J., Graule, T. and Baader, F., Ceramic forming using enzyme catalyzed reactions. *Mater. Chem. Phys.*, 1999, **61**(1), 78–102.
35. Tang, F., Fudouzi, H., Uchikoshi, T. and Sakka, Y., Preparation of porous materials with controlled pore size and porosity. *J. Eur. Ceram. Soc.*, 2004, **24**(2), 341–344.